Transactions on Additive Manufacturing Meets Medicine
Trans. AMMM, 2026, Vol. 8, No 1, Article ID 2435, 9 Pages

Infinite Science Publishing

Original Research Article

The efficacy of the inherent strain method in laser powder bed fusion for distortion compensation of removable partial dentures

C. P. Kloppers[1*] and D. de Beer[2]

[1] *North-West University, South Africa*
[2] *Centre for Rapid Prototyping and Manufacturing, Central University of Technology Free State, Bloemfontein, South Africa*
[*] *Corresponding author, email: cp.kloppers@nwu.ac.za*

Received August 11, 2025; **Accepted** April 20, 2026; **Published online** June 14, 2026

Abstract: Laser powder bed fusion (LPBF) is increasingly adopted in dentistry for the production of removable partial dentures (RPDs) and implant-supported RPDs (ISRPDs), offering advantages over conventional casting through digital workflow integration and reduced operator variability. However, thermally induced residual stresses during LPBF frequently cause distortion, compromising the geometric accuracy and clinical fit of these prostheses. This study investigates the efficacy of distortion compensation based on the inherent strain method implemented within a finite element framework. An orthotropic calibration procedure was developed using cantilever specimens manufactured parallel to the principal build directions. Distortion measurements were obtained using coordinate measurement machine (CMM) analysis following stress relief sectioning. Validation specimens were subsequently fabricated at 30° and 45° relative to the principal build direction to assess the predictive capability of the calibrated inherent strain model. The calibrated strain values were implemented in Simufact Additive to pre-distort digital mandibular and maxillary RPD geometries prior to fabrication. Geometrical deviations were quantified using intraoral scanning and comparison of predefined datum points between the nominal CAD models and as-built components. Distortion compensation resulted in a maximum local improvement of 410 µm and reduced mean maximum deviation by 23% and 27% for mandibular and maxillary frameworks, respectively, compared to uncompensated controls. The compensated dentures showed improved dimensional fidelity, with most deviations falling within clinically acceptable thresholds reported in recent literature, although localized deviations remained. The method demonstrated robustness across non-orthogonal build orientations and mesh refinements. These findings indicate that inherent strain-based distortion compensation can enhance the geometric accuracy of LPBF-fabricated dental prostheses and support improved integration of simulation-driven workflows in digital prosthodontics.

I. Introduction

Laser powder bed fusion (LPBF), an additive manufacturing (AM) technology, is used in applications as diverse as the automotive sector and aero-structures and is applied very successfully in the medical field [1,2]. The application of Cobalt-Chrome based alloys in the field of biomedicine and dentistry is well established as a biocompatible material. It has been used for decades [3,4,5,6]. Due to the materials that can be processed and the current limitations on the build size of typical LPBF units, manufacturing patient-specific implants such as maxilla, mandible, femur, and knee implants has become increasingly popular [7, 8, 9, 10, 11]. These implants and medical devices can be accurately manufactured with suitable material properties. AM presents a viable alternative to traditional manufacturing methods with the advantage of a digital workflow [12].

The application of AM in the clinical field of dentistry to facilitate solutions to tooth loss from a patient's dentition has been well studied. This disease is called edentulism [13, 14, 15, 16]. The rate of edentulism and partial edentulism in society and the age of patients experiencing this is a growing concern [17, 18]. Fagundes et al. have shown that the most privileged countries with better social

and public policies regarding healthcare have higher rates of edentulism [19]. Removable partial dentures (RPD) and implant-supported removable partial dentures (ISRPD) with distal extension have proven to be part of successful prosthetic rehabilitation for edentulous patients [20].

The use of LPBF to produce RPD and ISRPD structures has been studied widely. It has proven a viable alternative to lost wax casting, which was traditionally used [21]. LPBF has the further advantage of producing these geometrically complex structures with less dependency on operator variability and is significantly less operator-time intensive [22, 23, 24]. Boontherawara et al.'s recent study concluded that LPBF is more accurate in producing RPDs than conventional lost wax casting manufacturing techniques [25]. Although LPBF is a viable manufacturing method, the fit of the RPD to the patient's dentition has proven to be a critical aspect of ensuring successful rehabilitation [26].

Although some accommodation from the patient's side will be required when a new RPD or ISRPD is fitted, great care must be taken to include occlusal discrepancies and proper fitment of the prosthetic [27]. Heiba et al. compared the fit accuracy of RPD manufactured with direct milling and LPBF [28]. The authors found that direct milling accurately produced RPD to 189 µm, and selective laser melting could only achieve 456 µm in this study, quantified by an optical 3D scanning instrument. A different study by Arnold et al. found that LPBF produced RPD accurate to 363 µm but did not provide significant information regarding the LPBF parameters or pre-processing techniques employed [29]. A systematic review article published in 2023 indicated that RPD with internal discrepancies and overall accuracy of between 50 µm and 311 µm has been established to be clinically acceptable when comparing twenty-five different studies ranging from 2005 to 2022 [30]. It should be noted that reported accuracy values in these studies are defined using different metrics, including maximum deviation, mean deviation, root mean square (RMS] error, or internal gap measurements obtained from optical scanning or fit analysis. As a result, direct numerical comparison between studies must be interpreted with caution, and the reported ranges should be considered indicative rather than strictly equivalent.

Due to the spatially varied thermal cycles resulting from the LPBF build process, components such as RPD and ISRPD, when manufactured, are left with undesirable residual stress that can cause plastic deformation, resulting in an inaccurate fit [31, 32]. The residual stresses present in components produced by LPBF can affect corrosion resistance, fracture toughness and fatigue performance [32]. The inherent strain method has been implemented in LPBF to predict the residual stress resulting from the thermal history of the part and consequently predict the distortion of the part [33, 34]. The inherent strain method forms the basis for distortion compensation, where a component is pre-distorted to accurately resemble the required part dimensions when removed from the AM unit [35]. This method has been implemented by Gruber et al. on Inconel 718 when manufacturing stator vanes. It has been proven to produce parts accurately enough to comply with aerospace tolerances [36].

Modelling techniques to simulate the entire build process in a LPBF build environment have been developed to ensure that parts can be manufactured without defect, eradicating the trial and error method [37]. Mukalay et al. investigated the robustness of these modelling techniques in accurately predicting part distortion due to inherent strain. The authors found that Ansys Additive, COMSOL, Simufact Additive, Nettfab and Simulia provided good solutions [38]. These techniques enable the placement of parts and support structures within the LPBF unit to minimize the defects and inherent strains in the parts [39].

The aim of this study is to develop and evaluate an inherent strain-based distortion compensation workflow for LPBF-manufactured removable partial dentures (RPDs). It is hypothesised that:

(i) calibrated orthotropic inherent strain parameters can accurately predict distortion across multiple build orientations, and
(ii) application of these calibrated parameters to RPD frameworks reduces dimensional deviations to within clinically acceptable limits reported in the literature.

By integrating simulation-driven distortion compensation within a digital LPBF workflow, this study seeks to improve geometric fidelity and enhance the clinical viability of additively manufactured dental prostheses.

II. Material and methods

II.I. Materials

The material used in this study was a cobalt–chromium dental alloy powder (CO-538-1, Linde Advanced Material Technologies Inc., Indianapolis, IN, USA), certified in accordance with ASTM F75-18 (chemistry only).

The analysed lot contained 27.99 wt% Cr, 5.55 wt% Mo, 0.72 wt% Si, 0.67 wt% Mn, with cobalt as balance and minor elements within specification limits. Particle size distribution measured according to ASTM B822 showed a d50 of 32 µm (specified range 25–40 µm). Sieve analysis per ASTM B214 indicated 98–100% of particles below 325 mesh. The powder met Hall flow requirements per ASTM B213, with a measured flow time of 13 s.

Dental cobalt–chromium alloys used for removable partial dentures are typically specified according to ISO 22674 for metallic materials for fixed and removable restorations, and ASTM F75 for cast Co–Cr–Mo alloys.

II.II. Methods

This study aimed to determine the efficacy of the distortion compensation methods based on the inherent strain principle in the laser powder bed fusion additive manufacturing process. The components for this study were manufactured using the Olas Creator manufactured by OR-Laser GmbH. This laser powder bed fusion unit has a build envelope of 100 mm diameter and can produce parts up to 110 mm high. It is equipped with a 250W fibre laser with a z-axis resolution of 20 µm to100 µm. The manufacturing parameters used in this study are shown in Table 1.

Table 1: Manufacturing parameters

Parameter	Value
Layer Shift Angle	67°
Layer Height	25 µm
Contouring Laser Spot Size	40 µm
Contour Boundary Offset	80 µm
Contouring Power	140W
Mark Speed	250 mm/s
Hatching Spot Size	120 µm
Hatching Spot Overlap	50%
Hatching Boundary Offset	20 µm
Hatching Power	125W
Hatching Mark Speed	630 mm/s

Fabrication was performed using a layer-wise bidirectional hatch scanning strategy with a 67° hatch rotation between successive layers. A contour-first exposure strategy was employed; whereby external contour scans were completed prior to hatch infill exposure in each layer.

The platform was unheated, and no active preheating was applied during processing. Fabrication was conducted under a nitrogen shielding atmosphere (99.99% purity), maintained by the machine's controlled inert gas system. Oxygen levels were maintained below the manufacturer-specified operational threshold for LPBF processing. Support structures for the RPD frameworks were generated using the dental precision support module within 2BUILD software (2oneLab GmbH, Germany). The support design followed the software's standard dental precision model parameters for removable partial denture geometries.

Simufact Additive 2023.2 (MSC Software Corporation, Newport Beach, CA, USA) was used as finite element software in this study, applying the inherent strain and the subsequent distortion compensation method. Inherent strains caused by the thermal history of the part, as discussed by Mukalay et al. and Bihr et al., act as mechanical loads distorting the component when removed from the build plate [38, 39]. To effectively capture the behaviour of the inherent strain, a calibration process was carried out on cantilevers to quantify the inherent strain within the parts [37]. Accurate quantification of the distortion of the cantilevers was required as input to the calibration process to ensure accurate determination of the inherent strain. After the production of the cantilever, a horizontal cut was made in the component at a height of 2.9 mm from the base with an electrical discharge machining wire cutter, WEDM-HS with BKDK Controller, model number DK7732. The calibration cantilever specimen before and after sectioning is shown in Figure 1.

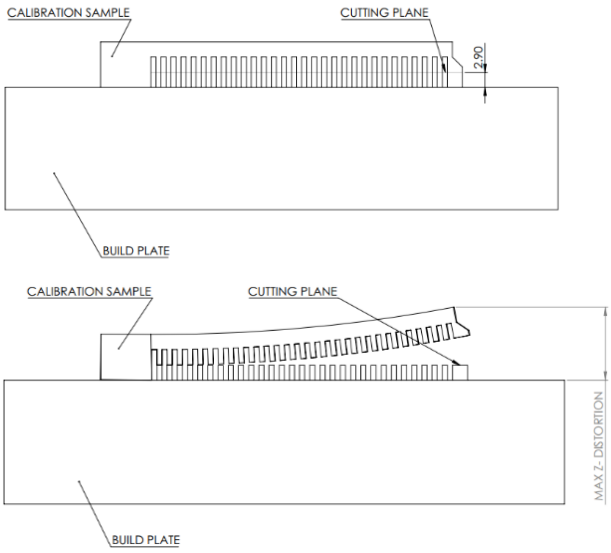

Figure 1: Calibration specimen before and after sectioning

The cut was made as soon as possible after the production of the parts to avoid any creep in the material due to the inherent strains present. The maximum distortion from this cantilever specimen was used to determine the inherent strain present using consecutive finite element modelling simulations. Due to their parametric shape, the cantilevers' distortion quantification was done using a coordinate-measuring machine (Hexagon Global Lite 07.07.05), as described by Liu et al., Dong et al. and Zhang et al. This has proven to be a solution to measure very accurately [34, 35, 40].

The Hexagon Global Lite 07.07.05 system has a maximum permissible error (MPEE) of (2.5 + L/300) µm in accordance with ISO 10360-2. Measurements were conducted using a 3 mm diameter ruby probe in touch-trigger mode. Each measurement location was probed once per specimen, and three locations across the cantilever width (left, mid, and right) were evaluated to determine mean distortion values. The measurement strategy focused on capturing maximum tip deflection following sectioning.

An orthotropic calibration was used to independently determine the inherent strain in the X-axis and the Y-axis. During the calibration simulation, the elements in the cutting plane were deactivated, resulting in a sectioned part. Thus, a mesh was chosen so that only a single row of elements was deactivated due to cutting. The cutting took place on the interface between two rows of mesh elements. Mesh sizes of 1mm, 0.5mm and 0.25mm were used during the calibration.

Two cantilever specimens were produced per orthotropic orientation, and mean distortion values were used for calibration [41]. All process parameters used to manufacture the calibration cantilevers, and all subsequent parts were kept constant to ensure accurate prediction of the inherent strains and the resulting distortion.

The validity of the calibration process was confirmed by validating the results. Simulations were performed on multiple cantilever specimens that were not manufactured at the orthotropic directions used in the calibration, parallel to the x-axis and the y-axis. These cantilevers were manufactured at 30°, 45° and 60° relative to the x-axis of the LPBF unit. They were subsequently cut in the same manner as the orthotropic cantilevers at a height of 2.9 mm from the base plate, and their distortion was quantified [36].

Custom RPD structures were designed for this study based on a generic set of dentures that did not contain patient-specific data. LPBF produced both a maxillary RPD and a mandibular RPD. Datum points were added to compare the CAD and additively manufactured RPD models. Simufact Additive was used to quantify the X, Y, and Z distances between the datum points on the CAD and the LPBF RPDs. A comparison of these geometries allowed for the quantification of the distortion present in the LPBF RPDs due to the thermal history of the parts.

For calibration purposes, two cantilever specimens were manufactured for each orthotropic orientation (horizontal and vertical). Similarly, two specimens were produced for each validation angle (30°, 45° and 60°). Mean distortion values were used for calibration and validation to reduce the influence of process-induced variability. Due to material and production constraints, the mandibular and maxillary RPD frameworks (compensated and uncompensated) were each manufactured once per condition. The primary objective of the RPD investigation was evaluation of distortion prediction capability rather than statistical assessment of process repeatability.

Due to the organic geometries of these components, Intra-Oral Scanning (IOS) has been identified as a valid method of quantifying shape and distortion. Intra-oral scanning is the most applicable technology in studies evaluating the trueness and accuracy of dental applications [42, 43, 44, 45]. Intraoral scanning was performed using a 3Shape TRIOS 5 system (3Shape A/S, Copenhagen, Denmark) operating under TRIOS Release 24.0 software. Scanned geometries were exported in STL format and imported into Simufact Additive 2023.2 (MSC Software Corporation, Newport Beach, CA, USA) for analysis. Alignment between scanned and reference CAD geometries was performed using the geometry inspection module within Simufact Additive, employing a best-fit alignment algorithm. Datum cylinders incorporated into the RPD designs were used as reference features, and measurements were manually extracted by evaluating the geometric centers of the cylindrical features.

Deviation analysis was performed on a point-based basis using maximum absolute deviation at each datum location. A global surface deviation metric such as root mean square (RMS) error was not calculated, as the study focused on discrete clinically relevant datum locations.

III. Results

Before attempting any distortion compensation, it was essential to calibrate the LPBF unit to ensure the accuracy of the experiments. Cantilevers with dimensions of 72 mm x 12 mm x 9 mm were manufactured using the laser parameters specified in Table 1. These cantilevers were then cut at a height of 2.9 mm above the datum plane to relieve the inherent strain. Distortion was quantified at three points across the width of the cantilever (left, middle, and right) to calculate an average and minimize the impact of potential outliers. The maximum deflection was measured at the very tip of the cantilever to accurately capture the distortion along the entire 72 mm length. The CMM quantified the distortion, and the results are presented in Table 2. The horizontal cantilevers produced perpendicular to the LPBF unit's inspection window were quantified at the point where maximum distortion is present and at three points over the width of the cantilever. The first sample has a maximum variation in the three measurement points of 13 µm, which is the most consistent of all the calibration samples. The left and right points on the cantilever differ by only 1 µm, with the midpoint being the lowest. The second sample produced in this orientation had a slope from left to right, with the left-most point being 17 µm higher than the rightmost point. In this case, the interesting phenomenon is the variation in the two samples relative to each other. The second sample distorted notably less than the first, with a variation between the two samples of 173 µm on average.

Table 2: CMM distortion results

Orientation	Specimen	Left [mm]	Mid [mm]	Right [mm]	Mean [mm]	Maximum variation [µm]
Horizontal	H1	2.271	2.251	2.242	2.255	29
	H2	2.282	2.266	2.265	2.271	17
Vertical	V1	2.818	2.813	2.819	2.817	13
	V2	2.654	2.642	2.637	2.644	17

The difference between vertical specimens was 173 µm, indicating orientation-dependent distortion behaviour. The first horizontal cantilever (printed parallel to the LPBF unit's inspection window) provided results indicative of a skewing from left to right; the variation over the width of the cantilever is 29 µm. The mean distortion of this cantilever only differed by 4 µm. When the second cantilever is produced in the same manner and with the same orientation as the first is compared, the left-most point is also the highest. This cantilever has a smaller variation within the measurement points with only a 17 µm difference. The most important aspect that needs to be highlighted is that there is only a 16 µm difference between the two cantilevers on average. This displays the repeatability of the production process and the quantification method.

As the software developer MSC Simufact Additive recommended, the average of these calibration cantilevers should be used during the calibration process to obtain a robust calibration model. The vertical samples thus had an average distortion of 2.7305 mm, and the horizontal samples had a distortion value of 2.2628 mm.

Orthotropic calibration was carried out within Simufact Additive using multiple mesh sizes. The mesh resolution was selected to balance geometric fidelity and computational efficiency. In voxel-based discretization, element size influences how accurately the part volume and boundary surfaces are represented. The chosen mesh therefore ensured stable global distortion prediction without introducing discretization artefacts. With the dimensions of the cantilever, three different mesh sizes were identified: 1.0 mm, 0.5 mm and 0.25 mm. These mesh sizes would result in accurate results without being computationally expensive.

A mesh sensitivity evaluation was performed to assess the influence of discretization on predicted distortion during the calibration process. The objective of this evaluation was not to establish strict asymptotic mesh convergence in the classical finite element sense, but rather to determine whether further mesh refinement produced meaningful changes in predicted distortion. Because the inherent strain method predicts macro-scale distortion using homogenized strain inputs rather than resolving local stress gradients, full convergence refinement is not required. Instead, the selected mesh must demonstrate numerical stability and negligible variation in predicted distortion with further refinement.

The calibration results for all investigated mesh sizes are summarised in Table 3. The 1.0 mm mesh achieved deviations below 6 µm. Refinement to 0.5 mm reduced deviations to below 1 µm for both orientations. Further refinement to 0.25 mm did not improve predictive accuracy despite significantly increased voxel count. Therefore, the 0.5 mm mesh was selected for subsequent validation and distortion compensation simulations.

The slight reduction in agreement observed with the 0.25 mm mesh is attributed to the nature of the inherent strain approach rather than numerical instability. The inherent strain method applies homogenized strain values to finite elements to reproduce macro-scale distortion behaviour. When the mesh is refined beyond a representative volume scale, the discretization no longer aligns optimally with the homogenized strain assumption, resulting in local stiffness redistribution and minor variations in predicted distortion. This effect does not indicate numerical divergence or instability but rather reflects the sensitivity of homogenized inherent strain inputs to element size. Consequently, further refinement beyond 0.5 mm did not provide additional predictive benefit while substantially increasing computational cost.

Validation of the calibration results is achieved by producing a sample that is not in the orthotropic directions and then determining if the simulation can accurately predict the distortion of the samples. Three validation cantilevers were produced at 30°, 45° and 60° relative to the horizontal sample produced parallel to the LPBF unit's inspection window.

Table 3: Comparison of mesh sizes during orthotropic calibration

Mesh Size [mm]	Orientation	Target [mm]	Simulation [mm]	Deviation [µm]	Calibration Steps
1.0	Horizontal	2.2628	2.2624	0.4	4
1.0	Vertical	2.7305	2.7251	5.3	4
0.5	Horizontal	2.2628	2.2635	0.4	6
0.5	Vertical	2.7305	2.7309	0.4	6
0.25	Horizontal	2.2628	2.2615	1.3	6
0.25	Vertical	2.7305	2.7057	2.4	6

It is crucial to ensure that as little time as possible lapses between the production of the sample and the cutting and the resulting measurement to ensure accurate and representative results. Table 4 displays the results obtained from the validation of these samples.

Table 4: Validation of inherent strain calibration

Build Angle	Predicted [mm]	Measured [mm]	Absolute Deviation [µm]
30°	2.039	2.166	127
45°	2.393	2.120	273
60°	2.030	2.133	102

The validation results showed good agreement between the simulated predictions and the experimental measurements. The 30° and 60° specimens exhibited deviations of 127 µm and 102 µm, respectively, while the 45° specimen showed the largest deviation of 273 µm.

Although the 45° case demonstrated a higher discrepancy, all deviations remained within the clinically acceptable range of 50–311 µm reported in the literature [30]. In addition, the deviations observed in this study are smaller than those reported in related studies evaluating the fit accuracy of RPD frameworks [28, 29]. These findings confirm that the orthotropic inherent strain calibration provides a reliable prediction of distortion for non-orthogonal build orientations.

The geometry of RPD and ISRPD is significantly more complex and organic than the calibration samples. The thin structures and complex geometry of RPD and ISRPD could lead to excessive distortion. A mandibular and maxillary denture produced by LPBF was manufactured to quantify the distortion when distortion compensation is applied.

To effectively investigate the effect of distortion compensation, a control sample was also fabricated to quantify the distortion of RPD and ISRPD that has not undergone distortion compensation. The quantification of geometries so complex is achieved by adding five datum points on each specimen distributed equally over the area of the samples.

These datum points consisted of a 1 mm diameter cylinder with a 45° chamfer to achieve the best possible quantification of the results. Figure 2 shows the dentures manufactured with and without the datum points present.

The results from quantifying the undistorted and distorted mandibular and maxillary dentures are presented below. The measurement points are numbered from left to right in an anticlockwise manner.

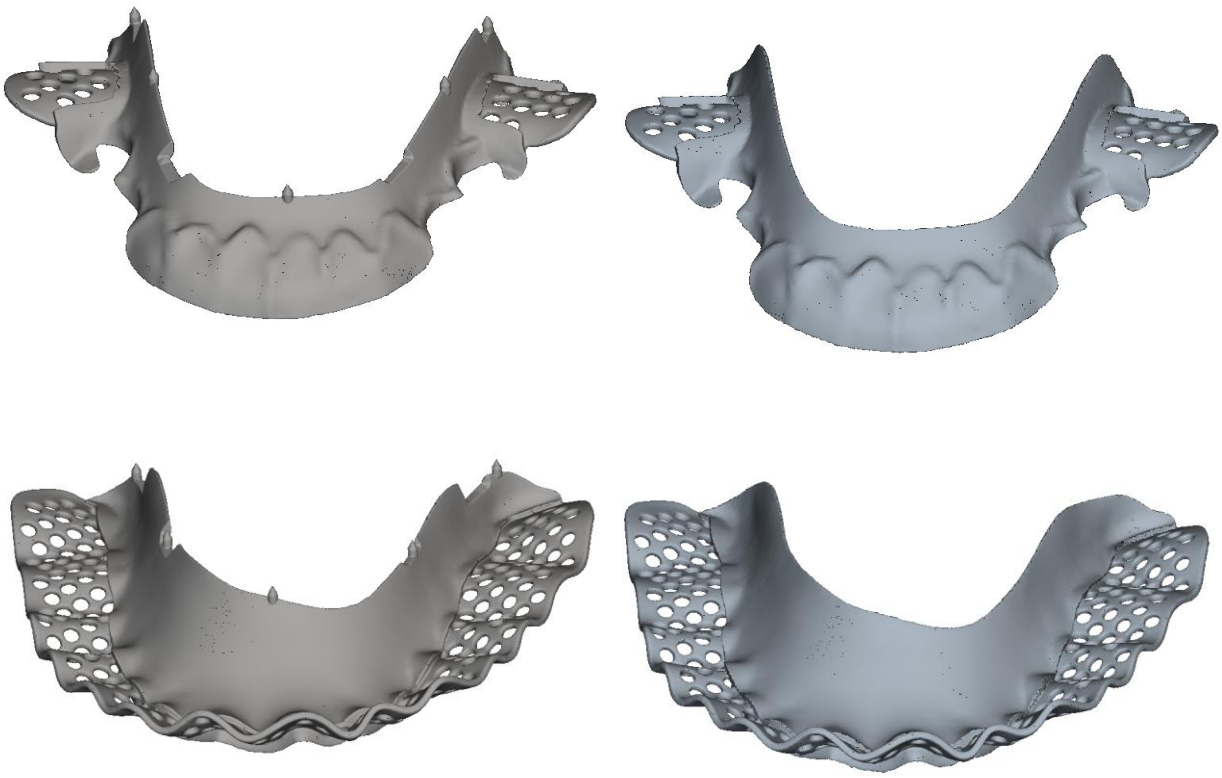

Figure 2: Mandibular and maxillary dentures with and without datum points.

Table 5: Mandibular denture – Absolute deviation

Point	Uncompensated [µm]	Compensated [µm]	Improvement [µm]
1	390	270	120
2	330	130	200
3	80	70	10
4	393	388	5
5	500	440	60
Mean	339	260	79
Maximum	500	440	200
RMS	366	283	
% Mean Improvement			23%

The distortion results presented in Table 5 represent the maximum absolute deviation at each measurement point. Distortion compensation reduced the mean maximum deviation from 339 µm to 260 µm, representing an average improvement of 79 µm. Four of the five measurement points demonstrated improved fit following compensation. The maximum deviation decreased from 500 µm in the uncompensated model to 440 µm in the compensated model. Although two points remained above the 311 µm clinical threshold, distortion compensation produced a clear overall improvement in fit accuracy. In addition to the reduction in mean deviation, RMS error decreased from 366 µm to 283 µm following distortion compensation, corresponding to a 23% improvement in mean deviation.

The highest deviations were consistently observed at distal extension regions corresponding to the clasp arms. These slender geometries exhibit reduced structural stiffness and are more susceptible to thermally induced distortion during LPBF processing.

Table 6: Maxillary denture – Absolute maximum deviation

Point	Uncompensated [µm]	Compensated [µm]	Improvement [µm]
1	300	150	150
2	240	150	90
3	233	368	-135
4	100	150	-50
5	430	130	300
Mean	261	190	71
Maximum	430	368	300
RMS	289	244	
% Mean Improvement			27%

Table 6 presents the maximum absolute deviation per measurement point for the maxillary denture. Distortion compensation reduced the mean maximum deviation from 261 µm to 190 µm, representing an average improvement of 71 µm. Three of the five measurement points showed improvement, while two points exhibited increased deviation after compensation. Nevertheless, the maximum deviation decreased from 430 µm to 368 µm, indicating an overall improvement in dimensional accuracy.

In the maxillary framework, increased deviation after compensation was primarily localized to posterior regions, suggesting geometry-dependent sensitivity of the compensation scaling to local stiffness variations.

Overall, distortion compensation resulted in improved fit accuracy compared to the uncompensated control samples. In all cases, the fit of the dentures compensated for the distortion caused by the thermal history of the part in the LPBF process demonstrated improved fit compared to the control sample.

IV. Discussion

The cantilever calibration successfully established orthotropic inherent strain parameters for the LPBF system investigated. The 0.5 mm mesh size provided an optimal balance between computational efficiency and predictive accuracy, with deviations below 1 µm during calibration. These calibrated inherent strain values are specific to the present LPBF configuration, including laser power, scan strategy, powder batch, layer thickness, and build atmosphere.

Validation using non-orthogonal cantilever orientations (30°, 45°, and 60°) demonstrated acceptable predictive capability, with deviations ranging from 102 µm to 273 µm. These values fall within the clinically acceptable internal discrepancy range of 50–311 µm reported in the systematic review by Rokhshad et al. [30]. The largest discrepancy was observed at 45°, suggesting orientation-dependent sensitivity in orthotropic parameter interpolation. Nevertheless, the results confirm that the inherent strain calibration captures the dominant distortion mechanisms of the LPBF process.

When applied to full RPD geometries, distortion compensation reduced the mean maximum deviation of the mandibular framework from 339 µm to 260 µm (23% improvement) and of the maxillary framework from 261 µm to 190 µm (27% improvement). These values compare favorably to previously reported LPBF RPD accuracies. Heiba et al. reported deviations of approximately 456 µm for LPBF, while Arnold et al. reported deviations around 363 µm [28, 29]. In contrast, the compensated frameworks in the present study demonstrate lower mean deviations and reduced maximum distortion, indicating that simulation-driven compensation can substantially improve dimensional fidelity beyond baseline LPBF performance reported in the literature.

Differences between studies may arise from several factors, including machine configuration, laser energy density, hatch rotation strategy, contouring sequence, powder characteristics, and geometric complexity. The present study employed a contour-first strategy with 67° hatch rotation and a nitrogen shielding atmosphere without active preheating. Variations in thermal gradients, residual stress accumulation, and support interaction can

significantly influence distortional behaviour. Therefore, direct numerical comparison between studies must be interpreted with consideration of these process-specific variables.

It is important to emphasize that inherent strain parameters are not universal material constants. They are machine- and process-dependent calibration parameters. Any modification in volumetric energy density, scan strategy, layer thickness, hardware configuration, or powder characteristics would require re-calibration. This dependency represents both a limitation and a strength of the approach: while calibration must be repeated when process conditions change, once established, it provides a computationally efficient and robust method for distortion prediction and compensation.

From a practical perspective, the integration of inherent strain-based compensation into a digital LPBF workflow offers significant potential benefits for dental laboratories. By reducing post-processing adjustment and chairside modification time, improved geometric fidelity may enhance prosthetic fit and reduce clinical intervention. However, laboratories adopting such workflows must implement controlled calibration procedures and maintain process stability to ensure predictive reliability.

Although distortion compensation improved overall dimensional accuracy, certain regions, particularly distal extension and clasp areas, remained sensitive to local stiffness variations. This indicates that geometry-specific compensation scaling or adaptive regional compensation strategies may further enhance accuracy in future work.

Limitations of this study include the use of a single material batch, a single LPBF machine configuration, and single-production RPD specimens per condition. Additionally, evaluation was based on discrete datum measurements rather than full-field deviation mapping. Future investigations should incorporate larger sample sizes, alternative scanning strategies, stress-relief treatments, and full-surface deviation analysis to further validate the robustness of inherent strain-based compensation in clinical dental applications.

V. Conclusion

This study demonstrated that orthotropic inherent strain calibration within a finite element framework can reliably predict distortion in LPBF-manufactured cobalt–chromium removable partial dentures. Calibration using cantilever specimens yielded stable inherent strain parameters, and validation at non-orthogonal build orientations (30°, 45°, and 60°) showed predictive deviations between 102 µm and 273 µm, confirming the robustness of the modelling approach.

Application of simulation-driven distortion compensation reduced the mean maximum deviation from 339 µm to 260 µm (23% improvement) for the mandibular framework and from 261 µm to 190 µm (27% improvement) for the maxillary framework. While certain localized regions remained above the 311 µm clinical threshold reported in the literature, overall dimensional fidelity was measurably improved following compensation.

The calibrated inherent strain parameters are process-dependent and specific to the LPBF configuration used in this study, including laser parameters, scan strategy, powder characteristics, and machine setup. Any significant modification to these conditions would require re-calibration.

Limitations of this work include the use of a single machine configuration, a single material batch, and single RPD specimens per condition. Furthermore, dimensional evaluation was based on discrete datum measurements rather than full-field deviation mapping.

Future research should investigate larger sample sets, adaptive geometry-dependent compensation strategies, alternative scan strategies, stress-relief treatments, and patient-specific clinical validation. Integration of full-surface deviation analysis and compensation scaling optimisation may further enhance predictive accuracy.

Overall, inherent strain-based distortion compensation provides a practical and computationally efficient strategy for improving geometric fidelity in LPBF-fabricated dental prostheses and supports the broad.

Author's Statement

Conflict of interest: The authors state no conflict of interest. Animal models: Indicate here under which approval you have carried out animal experiments. Informed consent: Informed consent has been obtained from all individuals included in this study. Ethical approval: The research related to human use complies with all the relevant national regulations, institutional policies and was performed in accordance with the tenets of the Helsinki Declaration, and has been approved by the authors' institutional review board or equivalent committee.

References

[1] N. Zhao N, M. Parthasarathy M, S. Patil S, D. Coates D, K. Myers K, H. Zhu H, et al., Direct additive manufacturing of metal parts for automotive applications,. Journal of Manufacturing Systems. 2023;, 68 (2023) 368-75.

[2] K. Morshed-Behbahani, A. Aliyu, D. P. Bishop, A. Nasiri, Additive manufacturing of copper-based alloys for high-temperature aerospace applications: A review, Materials Today Communications 38 (2024).

[3] D. Viderščak, Z. Schauperl, M. Godec, Č. Donik, I. Paulin, M. Šercer, et al., Influence of laser powder bed fusion parameters on microstructure and mechanical properties of Co–Cr dental alloy, Journal of Materials Research and Technology 30 (2024) 6218-26.

[4] A. Raza, K. M. Deen, E. Asselin, W. Haider, TK diagrams to determine the impact of pH variation on 3D printed CoCr alloy implant corrosion, Journal of Electroanalytical Chemistry (2023) 929.

[5] M. Isik, J. D. Avila, A. Bandyopadhyay, Alumina and tricalcium phosphate added CoCr alloy for load-bearing implants, Addit Manuf. 36 (2020).

[6] B. Singh, G. Singh, B. S. Sidhu, In vitro investigation of Nb Ta alloy coating deposited on CoCr alloy for biomedical implants. Surface and Coatings Technology (2019) 377.

[7] C. Van den Borre, M. Rinaldi, B. De Neef, N. A. J. Loomans, E. Nout, L. Van Doorne, et al. Patient- and clinician-reported outcomes for the additively manufactured sub-periosteal jaw implant (AMSJI) in the maxilla: a prospective multicentre one-year follow-up study, Int J Oral Maxillofac Surg. 51(2) (2022) 243-50.

[8] L. A. Vaira, A. Biglio, A. Favro, G. Salzano, V. Abbate, J. R. Lechien, et al. Implant-prosthetic rehabilitation of the atrophic posterior mandible with additively manufactured custom-made subperiosteal implants: a cohort study. Int J Oral Maxillofac Surg. 53(6) (2024) 533-40.
[9] R. Rakesh Reddy, K. Jaya Prakash, S. Koteswari, A. Ud, B. Srinivasa Prasad, Y. S. Narayan, Additive manufacturing of a human mandible and finite element analysis of dental implant for prosthodontic applications, Materials Today: Proceedings 45 (2021) 3028-35.
[10] P. Kumar, M. S. Sawant, N. K. Jain, S. Gupta, Study of mechanical characteristics of additively manufactured Co-Cr-Mo-2/4/6Ti alloys for knee implant material, CIRP Journal of Manufacturing Science and Technology 39 (2022) 261-75.
[11] P. Kumar, M. S. Sawant, N. K. Jain, S. Gupta, Microstructure characterization of Co–Cr–Mo–xTi alloys developed by micro-plasma based additive manufacturing for knee implants, Journal of Materials Research and Technology 21 (2022) 252-66.
[12] G. Cakmak, J. Chebaro, M. B. Donmez, D. Yilmaz, H. I. Yoon, C. Kahveci, et al., Influence of intraoral scanner and finish line location on the fabrication trueness and margin quality of additively manufactured laminate veneers fabricated with a completely digital workflow. J Prosthet Dent. 131(2) (2024) 313 e1- e9.
[13] M. Silva, R. Felismina, A. Mateus, P. Parreira, C. Malça, Application of a Hybrid Additive Manufacturing Methodology to Produce a Metal/Polymer Customized Dental Implant, Procedia Manufacturing 12 (2017)150-5.
[14] K. Ma, H. Chen, Y. Shen, Y. Guo, W. Li, Y. Wang, et al., Feasibility study and material selection for powder-bed fusion process in printing of denture clasps. Comput Biol Med. 157 (2023) 106772.
[15] V. A. P. Chia, Y. L. See Toh, H.C. Quek, Y.cPokharkar, A. U. Yap, N. Yu, Comparative clinical evaluation of removable partial denture frameworks fabricated traditionally or with selective laser melting: A randomized controlled trial, J Prosthet Dent. 131(1) (2024) 42-9.
[16] W. Xie, M. Zheng, J. Wang, X. Li, The effect of build orientation on the microstructure and properties of selective laser melting Ti-6Al-4V for removable partial denture clasps, J Prosthet Dent.123(1) (2020) 163-72.
[17] W. L. See, T. L. Khoo, M. Mohan, S. Nimbalkar, P. G. Patil, Effect of surgical and prosthodontic protocols of distal extension implant-supported removable partial dentures on clinical and patient-reported outcomes: A systematic review, J Prosthet Dent. (2024).
[18] R. Borg-Bartolo, A. Roccuzzo, P. Molinero-Mourelle, M. Schimmel, K. Gambetta-Tessini, A. Chaurasia, et al., Global prevalence of edentulism and dental caries in middle-aged and elderly persons: A systematic review and meta-analysis, J Dent. 27 (2022) 104335.
[19] M. L. B. Fagundes, O. Junior, F. N. Hugo, N. J. Kassebaum, J. Giordani, Distribution of Edentulism by the Macro Determinants of Health in 204 Countries and Territories: An Analysis of the Global Burden of Disease Study. J Dent. 146 (2024) 105008.
[20] G. Talmazov, J. Young, D. Thomas, P. L. Michaud, A technique to guide implant placement with the long axis parallel to the path of insertion of removable partial dentures. J Prosthet Dent. (2023).
[21] L. Dolfini Alexandrino, L. H. Martinez Antunes, A. L. Jardini Munhoz, A. P. Ricomini Filho, W. J. da Silva, Mechanical and surface properties of Co-Cr alloy produced by additive manufacturing for removable partial denture frameworks. J Prosthet Dent. 130(5) (2023) 780-5.
[22] S. Yager, J. Ma, H. Ozcan, H. I. Kilinc, A. H. Elwany, I. Karaman, Mechanical properties and microstructure of removable partial denture clasps manufactured using selective laser melting, Additive Manufacturing 8 (2015) 117-23.
[23] Y. Kajima, A. Takaichi, T. Nakamoto, T. Kimura, Y. Yogo, M. Ashida, et al., Fatigue strength of Co-Cr-Mo alloy clasps prepared by selective laser melting, J Mech Behav Biomed Mater 59 (2016) 446-58.
[24] J. Sun, F. Q. Zhang The application of rapid prototyping in prosthodontics, J Prosthodont, 21(8) (2012) 641-4.
[25] P. Boontherawara, P. Chaijareenont, P. Angkasith, Comparing the trueness of 3D printing and conventional casting for the fabrication of removable partial denture metal frameworks for patients with different palatal vault depths: An in vitro study, J Prosthet Dent. (2024).
[26] R. J. Williams, R. Bibb, D. Eggbeer, J. Collis, Use of CAD/CAM technology to fabricate a removable partial denture framework, J Prosthet Dent. 96(2) (2006) 96-9.
[27] A. B. Carr, D. T. Brown, McCrackens's Removable Partial Prosthodontics, 12th ed., 2011.
[28] I. M. Heiba , S. L. Mohamed, M. E. Sabet, Accuracy and surface roughness of Co-Cr partial denture frameworks with different digital fabrication methods, J Prosthet Dent. 131(3) (2024) 520 e1- e7.
[29] C. Arnold, J. Hey, R. Schweyen, J. M. Setz, Accuracy of CAD-CAM-fabricated removable partial dentures, J Prosthet Dent. 119(4) (2018) 586-92.
[30] R. Rokhshad, A. Mazaheri Tehrani, A. Zarbakhsh, M. Revilla-Leon, Influence of fabrication method on the manufacturing accuracy and internal discrepancy of removable partial dentures: A systematic review and meta-analysis, J Prosthet Dent. (2023).
[31] A. Shrivastava, S. Anand Kumar, S. Rao, A numerical modelling approach for prediction of distortion in LPBF processed Inconel 718, Materials Today: Proceedings 44 (2021) 4233-8.
[32] T. Mukherjee, W. Zhang, T. DebRoy, An improved prediction of residual stresses and distortion in additive manufacturing, Computational Materials Science 126 (2017) 360-72.
[33] Z. D. Zhang, O. Ibhadode, S. I. Shahabad, X-Y. Zhai, D-Y. Yu, T. Gao, et al., High-resolution inherent strain method using actual layer thickness in laser powder bed fusion additive manufacturing with experimental validations, Journal of Materials Research and Technology 30 (2024) 6576-95.
[34] M. Zhang, C. Ji, Y. Hou, P. Jin, J. He, J. Wu, et al., Modified inherent strain method coupled with shear strain and dynamic mechanical properties for predicting residual deformation of Inconel 738LC part fabricated by laser powder bed fusion, International Journal of Thermal Sciences 203 (2024).
[35] W. Dong, B. J. Paudel, H. Deng, S. Garner, A. C. To, Data-driven distortion compensation for laser powder bed fusion process using Gaussian process regression and inherent strain method, Materials & Design (2024) 243.
[36] K. Gruber, G. Ziółkowski, A. Pawlak, T. Kurzynowski, Effect of stress relief and inherent strain-based pre-deformation on the geometric accuracy of stator vanes additively manufactured from inconel 718 using laser powder bed fusion, Precision Engineering 76 (2022) 360-76.
[37] M. R. Khosravani, P. Soltani, T. Reinicke, On the modeling of additive manufacturing: Printing process and printed structures, Mechanics Research Communications (2023) 131.
[38] T. A. Mukalay, J. A. Trimble, K. Mpofu, R. Muvunzi, Selective laser melting: Evaluation of the effectiveness and reliability of multi-scale multiphysics simulation environments,Heliyon 10(4) (2024) e25706.
[39] M. Bihr, G. Allaire, X. Betbeder-Lauque, B. Bogosel, F. Bordeu, J. Querois, Part and supports optimization in metal powder bed additive manufacturing using simplified process simulation, Computer Methods in Applied Mechanics and Engineering 395 (2022).
[40] W. Liu, X. Chen, W. Zeng, W. Sun, D. Gorman, A. Wilson, et al., Comparison of X-ray computed tomography and coordinate-measuring system dimensional measurement for additive manufacturing parts using physical and simulation methods, Measurement (2024) 229.
[41] U. P. Singh, S. Swaminathan, G. Phanikumar, Thermo-mechanical approach to study the residual stress evolution in part-scale component during laser additive manufacturing of alloy 718, Materials & Design (2022) 222.
[42] A. Grymak, A. Badarneh, S. Ma, J. J. E. Choi, Effect of various printing parameters on the accuracy (trueness and precision) of 3D-printed partial denture framework, J Mech Behav Biomed Mater 140 (2023) 105688.
[43] A. F. Neena, M. E. Abd-Ellah, Trueness of artificial teeth for CAD-CAM complete dentures fabricated with additive manufacturing implementing different denture base-tooth offset values: An in vitro study, J Prosthet Dent 131(4) (2024) 705 e1- e7.
[44] W. J. Lee, Y. H. Jo, B. Yilmaz, H. I. Yoon, Effect of layer thickness, build angle, and viscosity on the mechanical properties and manufacturing trueness of denture base resin for digital light processing, J Dent. 135 (2023)104598.
[45] Y. Tian, C. Chen, X. Xu, J. Wang, X. Hou, K. Li, et al., A review of 3D printing in dentistry: Technologies, affecting factors, and applications, Scanning (2021) 9950131.
[1] G. O. Young, *Synthetic structure of industrial plastics* (Book style with paper title and editor), in Plastics, 2nd ed. vol. 3, J. Peters, Ed. New York, McGraw-Hill, 1964, pp. 15–64.
[2] W.-K. Chen, Linear Networks and Systems (Book style). Belmont, CA: Wadsworth, 1993, pp. 123–135.
[3] J. U. Duncombe, Infrared navigation—Part I: An assessment of feasibility (Periodical style), IEEE Trans. Electron Devices, vol. ED-11, pp. 34–39, Jan. 1959.